Effects of V and Co Element Addition on Microstructures and the Mechanical Properties of In Situ Biphasic Hybrid (TiC$_x$N$_y$–TiB$_2$)/Ni Cermets

Feng Qiu [1,2,3,4] (ID)**, Xiangzheng Duan** [1,2,3]**, Xiujuan Li** [1,2,3,*] (ID)**, Hongyu Yang** [5] **and Yawei Wang** [2,3]

[1] Key Laboratory of Bionic Engineering, Ministry of Education, Jilin University, Changchun 130025, Jilin, China; qiufeng@jlu.edu.cn (F.Q.); duanxz17@mails.jlu.edu.cn (X.D.)
[2] Key Laboratory of Automobile Materials, Ministry of Education, Jilin University, Changchun 130025, Jilin, China; ywwang@mails.jlu.edu.cn
[3] Department of Materials Science and Engineering, Jilin University, Changchun 130025, Jilin, China
[4] Qingdao Automotive Research Institute of Jilin University, Qingdao 266000, Shandong, China
[5] School of Materials Science and Engineering, Jiangsu University of Science and Technology, Zhenjiang 212003, Jiangsu, China; yanghy@just.edu.cn
[*] Correspondence: xiujuanli@jlu.edu.cn; Tel.: +86-431-8509-5760

Abstract: In situ micro-(TiC$_x$N$_y$–TiB$_2$)/Ni cermets with different Co and V content (2,5 and 8 wt.%) were successfully fabricated by combustion synthesis and hot press consolidation in Ni–(V/Co)–Ti–B$_4$C–BN systems. The results indicate that as Co content increased from 0 to 8 wt.%, the average sizes of the ceramic particles decreased, when the content of V increased from 0 to 8 wt.%, the size of the ceramic particles first decreased and then increased, and when the V content is 5%, the ceramic particle size is the smallest. The Co element did not participate in the SHS reaction and was a diluent; therefore, when the Co element was added, the combustion temperature continued to decrease. When the V content was no more than 5 wt.%, as the V content increased, the maximum combustion temperature decreased. When the content of V was less than 5 wt.%, the concentration of V was not sufficient to greatly promote the generation of VN. Therefore, V absorbed a large amount of heat during the reaction, resulting in a continuous decrease in the reaction temperature of the reaction system during the reaction. When the content of the added V continued to increase to 8 wt.%, V participated in the reaction, which was exothermic. The results indicate that as Co content increased from 0 to 8 wt.%, the average sizes of the ceramic particles decreased, and the cermets with 5 wt.% Co possessed the best comprehensive properties: the highest hardness (1967 Hv), superior compression strength (3.25 GPa) and higher fracture strain (3.3%). Correspondingly, when the V content was 8 wt.%, the ultimate compressive strength and hardness of the cermets reached 1823 Hv and 3.11 GPa, respectively, 262 Hv and 0.17 GPa higher than those of the unalloyed cermets, respectively. Furthermore, the effects of Co and V on strengthening mechanisms were analyzed.

Keywords: combustion; in situ; cermets; compression property

1. Introduction

In recent years, with the development of the aerospace, automotive, exploration and mining industries, higher requirements have been placed on the performance of materials. In the aviation field, the thrust-to-weight ratio is an engine's core parameter and directly affects an aircraft's various indicators [1,2]. As the thrust and efficiency of the engine increase, the engine's turbine inlet increases, as do the requirements for high-temperature and corrosion-resistant materials [3,4]. Among the tool materials in the exploration industry, the current high-speed and high-efficiency cutting tools are

mainly superhard tools (including ceramics, diamond and cubic boron nitride (CBN)) and cermet tools [5–8]. The materials used to prepare such tools require high hardness, high wear resistance, sufficient strength and toughness, high heat resistance and good processability and economy. Ceramic matrix cermets have a high melting point, stiffness and hardness and are resistant to creep and fatigue [9–12]. This not only helps to overcome the high density and low temperature resistance of metal materials, but also surmounts shortcomings such as the brittleness of structural ceramics [13–15]. Therefore, ceramic matrix cermets have become the research focus of relevant scholars in recent years. TiB_2 and TiC_xN_y ceramics are widely used in the preparation of electrodes and cutting tools because of their high hardness, high modulus, high electrical conductivity, high melting point, low density and excellent chemical stability [16–18]. In addition, the compression performance and wear resistance of two-phase ceramic particle reinforced cermets are higher for single-phase ceramic particle reinforced composites [19,20]. Ni has excellent plasticity, ductility and impact resistance and high temperature and corrosion resistance, and the wettability between Ni and ceramic phase is good [21]. Therefore, Ni as a binder with biphasic ceramics as the matrix of cermets has better strength, hardness, wear resistance, oxidation resistance and adhesion resistance [22–24]. At present, many studies and reports have considered Ni-based composites with TiC_x, TiB_2 and TiC_xN_y as single-phase reinforcements [25]. Furthermore, the addition of alloying elements can change the wettability of ceramic particles and matrices, which can affect the density and microstructure and change the hardness, strength and toughness of the cermets [26–30]. The current research on the addition of alloying elements concentrates mostly on molybdenum and tungsten; few studies have considered the addition of Co and V in examining the microstructure and properties of cermets [31]. Co and V are metal elements with a high melting point. Study of the effects of the addition of Co and V elements on ceramic particle size, interface binding, element distribution and the mechanical properties of $(TiC_xN_y+TiB_2)$/Ni cermets prepared by in situ reaction of the Ni–Ti–B_4C–BN system [32–36] and analysis of the differences between the influence of the two elements have important value and significance [37–40].

In this study, the Ni–Ti–B_4C–BN system was selected as the research object. Hybrid $TiC_xN_y+TiB_2$/Ni cermets were prepared by a combined combustion synthesis and hot-pressing method. The effects of Co and V contents on the ceramic particle size, interface binding, element distribution and mechanical properties of $(TiC_xN_y+TiB_2)$/Ni cermets were investigated.

2. Experimental Procedures

Figure 1 is a schematic diagram of the preparation principle of the TiC_xN_y–TiB_2/Ni cermets. The raw materials used were commercial Ni powders (99.7 wt.% purity, ~25 μm in diameter, Beijing nonferrous metals research institute, Beijing, China), titanium powders (99.5 wt.% purity, ~58 μm in diameter, Beijing nonferrous metals research institute, Beijing, China), BN powders (99.3 wt.% purity, ~3 μm in diameter, Liaobin chemical company, Yingkou, Shandong, China), B_4C powders (99.3 wt.% purity, ~3.5 μm in diameter, Zhengxing abrasive company, Dunhua, Jilin, China), Co powders (99.5 wt.% purity, ~47 μm in diameter, Beijing nonferrous metals research institute, Beijing, China) and V powders (99.7 wt.% purity, ~47 μm in diameter, Beijing nonferrous metals research institute, Beijing, China). As shown in Figure 1a,b, high-energy ball milling (Gosta, Siping, Jilin, China) was used to activate the boron carbide and boron nitride powders (Beijing nonferrous metals research institute, Beijing, China)at a rating speed of 200 r/min. The mole ratio of Ti:B_4C:BN was fixed at 9:2:2, corresponding to the reaction in Equation (1).

$$9Ti + 2B_4C + 2BN \rightarrow 4Ti(C_{0.5}N_{0.5}) + 5TiB_2 \tag{1}$$
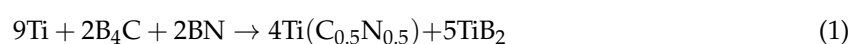
Co and V powders at weight percentages of 2, 5 and 8 wt.% were added to the mixed powders ceramic particles at 70 wt.%, and the mixed powders were mixed with a stainless steel mixer (Gosta, Siping, Jilin, China) at a low speed (50 r/min) for 8 h, as shown in Figure 1c. The powders were pressed into a cylindrical shape on a cold press. The sample was then placed in a vacuum thermal explosion furnace

(Gosta, Siping, Jilin, China), as shown in Figure 1e, and heated at a rate of 30 °K/min under vacuum. A sharp increase in barometric pressure indicated that the sample had reacted. The pressure was immediately applied to the sample for 60 s. Finally, the $(TiC_xN_y–TiB_2)$/Ni cermets were successfully obtained by cooling to room temperature.
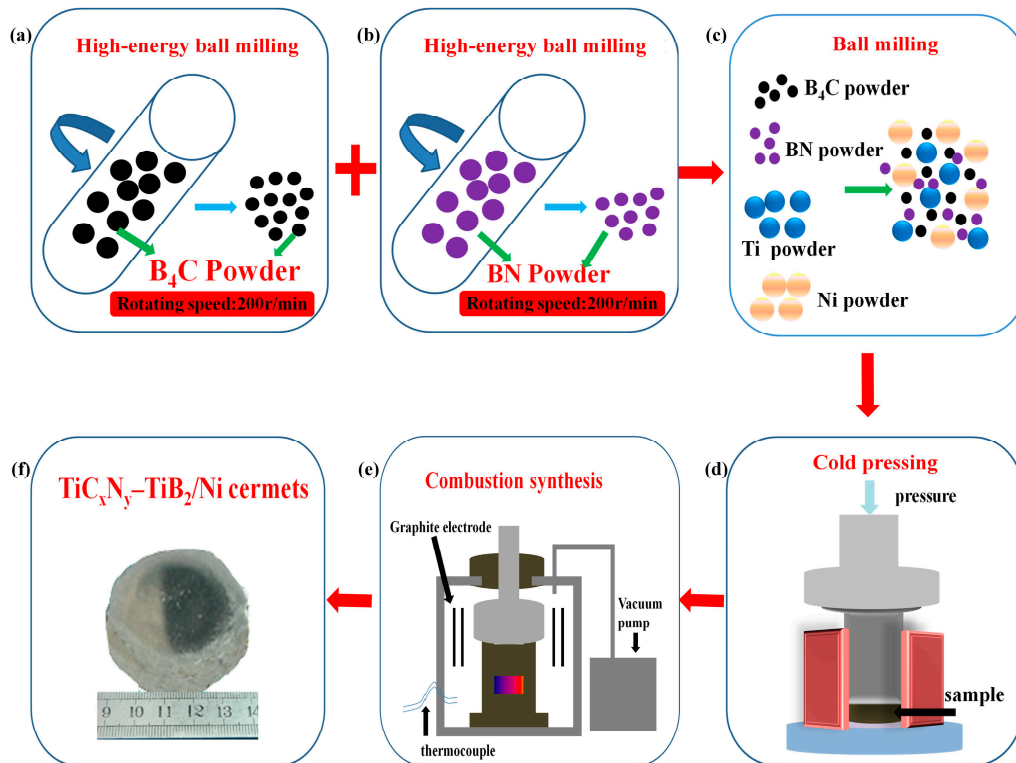

Figure 1. Schematic diagram of the preparation principle of the $(TiC_xN_y–TiB_2)$/Ni cermets. (**a**) High-energy ball milling of B_4C powder. (**b**) High-energy ball milling of BN powder. (**c**) Ball milling treatment of mixed powders. (**d**) Cold pressing mixed powders into a cylinder. (**e**) Preparation of micro-sized $(TiC_xN_y–TiB_2)$/Ni cermets by hot press sintering of the compacts. (**f**) Sample of $(TiC_xN_y–TiB_2)$/Ni cermets.

The SHS experiment was carried out under a vacuum vessel (Qikun science, Hangzhou, zhejiang, China) in an Ar atmosphere. Figure 2 shows the schematic diagram of the device for the SHS experiment. In this experiment, arc heating was used, and the current of the arc welding was 85 A. The temperature of the sample was measured by W5–Re25 thermocouples (Kaitai, Shanghai, China). During the sample reaction, the data measured by the thermocouples were recorded and processed by a computer acquisition system (Hewlett-Packard development company, Changchun, Jilin, China).

The phase constituent of the sample was investigated by X-ray diffraction (XRD, Model D/Max 2500PC Rigaku, Tokyo, Japan) with Cu Kα radiation. The microstructure was investigated via scanning electron microscopy (SEM, Model Evo18 Carl Zeiss, Oberkochen, Germany). Density was measured by the drainage method according to the Archimedes principle. A servo-hydraulic materials testing system (MTS, MTS 810, Minneapolis, MN, USA) was applied to the compression test with a strain rate of 1×10^{-4} s^{-1} at room temperature. Cylindrical specimens with a diameter of 3 mm and a height of 6 mm were used for the compression tests. A Vickers hardness tester (Model 1600-5122VD, Laizhou, Shandong, China) was used to test the microhardness of the cermets. The standard Charpy impact test was conducted using a semiautomatic impact tester (JBW-300B, JNKH, Jinan, Shandong, China).
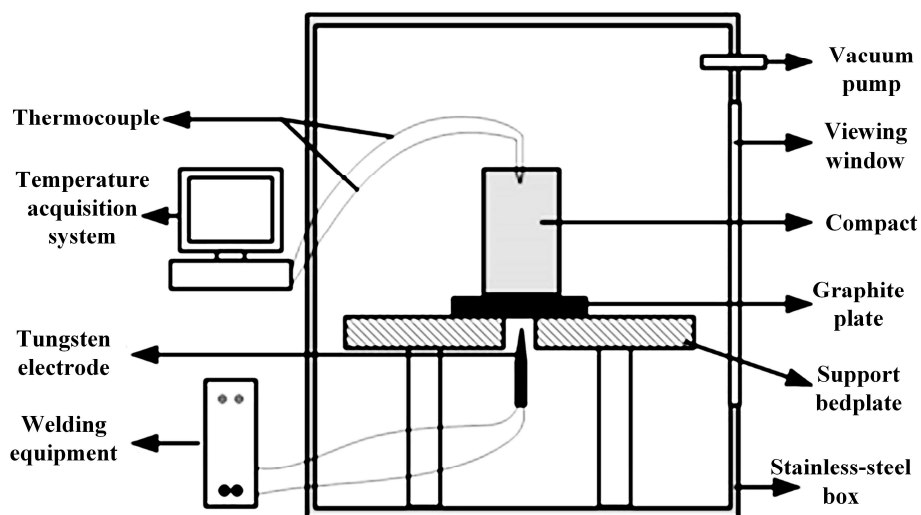
Figure 2. Self-propagating high-temperature synthesis (SHS) experimental device schematic.

3. Results and Discussion

Figure 3a shows XRD patterns for the $(TiC_xN_y–TiB_2)/Ni$ cermets with 0, 2, 5 and 8 wt.% Co addition. When Co was not added, the products contained only TiB_2, TiC_xN_y and Ni phases. After the addition of Co, only a small amount of $Ni_{20}Ti_3B_6$ phase appeared, and the other phases did not change. Therefore, the addition of Co had no effect on the cermet reaction. Figure 3b shows the XRD patterns for the $(TiC_xN_y–TiB_2)/Ni$ cermets with 0, 2, 5 and 8 wt.% V addition. When V was not added, the products in the system were relatively pure, containing only TiB_2, TiC_xN_y and Ni phases. As the content of V increased from 2 to 5 wt.%, $Ni_{20}Ti_3B_6$ and Ni_3Ti phases appeared one after the other. When the V content continued to increase to 8 wt.%, in addition to Ni, TiB_2, TiC_xN_y and $Ni_{20}Ti_3B_6$, a new phase, VN, appeared. This indicates that as the content of V increased, the reaction of $Ni–V–Ti–B_4C–BN$ system was not complete, and incomplete reactant and intermediate phases appeared successively. When the V content was increased to a certain extent, a large number of VN phases appeared in the system. Similar results were reported by Wang [41,42]. In the $(TiC_xN_y–TiB_2)/Ni$ composites without the addition of W, only the Ni, TiC_xN_y and TiB_2 phases are detected, while in the composites with the addition of W, a few $Ni_{20}Ti_3B_6$ and Ni_3Ti phases can be detected. It can be explained by the decline in the combustion temperature of the systems, which will be discussed below. Therefore, the addition of V, Co and W elements in the $Ni–Ti–B_4C–BN$ system causes incomplete reaction.

Figure 4 shows the microstructures of the $(TiC_xN_y–TiB_2)/Ni$ cermets with different Co and V contents. Figure 5 shows the size distribution diagrams of ceramic particles in the $(TiC_xN_y–TiB_2)/Ni$ cermets with different Co and V contents. As shown in Figure 4b–d, the ceramic particle size in the alloy did not change much, indicating that the Co content had little effect on the ceramic particle change. Figure 4e–g show energy-dispersive spectra (EDS) of $(TiC_xN_y–TiB_2)/Ni$ cermets with different Co contents. The white phase was a Co-rich phase. As the Co content increased, the enrichment zone of Co increased. Co did not participate in the reaction and acted only as a diluent, so it could only reduce the maximum combustion temperature of the reaction system to a smaller extent than the Group VIB alloying elements. As the Co content increased, the size of the ceramic particles was gradually reduced, as shown in Figures 5b–d and 6.
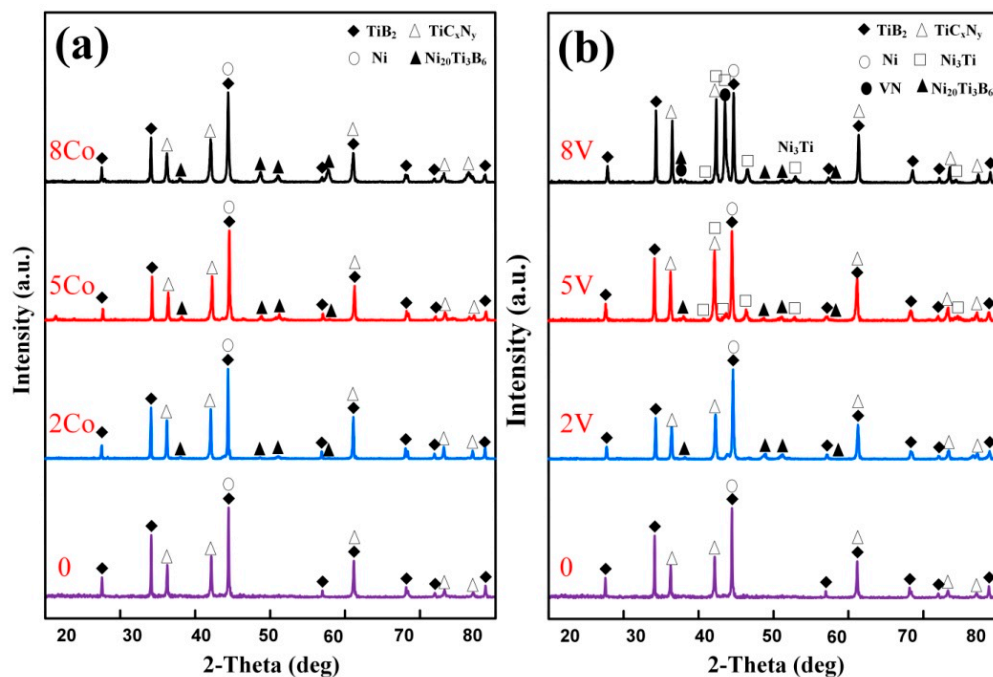
Figure 3. X-ray diffraction patterns for the (TiC_xN_y–TiB_2)/Ni cermets. (**a**) (TiC_xN_y–TiB_2)/Ni cermets with different Co contents (Co content from bottom to top is 0, 2, 5 and 8 wt.%, respectively). (**b**) (TiC_xN_y–TiB_2)/Ni cermets with different V contents (V content from bottom to top is 0, 2, 5 and 8 wt.%, respectively).

Figure 4h–j shows the SEM images of the (TiC_xN_y–TiB_2)/Ni cermets with different V contents. The ceramic particles in the (TiC_xN_y–TiB_2)/(Ni+V) cermets were uniformly distributed. The size of the ceramic particles decreased first and then increased with the increase in V content, as shown in Figure 5e–g. When the V content was 5 wt.%, the ceramic particle size was at least 1.42 μm. With the addition of W and Al, and the sizes of the ceramic particles also decrease to less than 2 μm [42,43]. Figure 6 shows a statistical plot of the average size of ceramic particles with different amounts of Co and V cermets. The alloying element increased from 0 to 5wt.%, and the refinement effect of V on ceramic particles was more significant. When the V and Co contents were continuously increased to 8 wt.%, the ceramics in the cermets in which the Co and V elements were respectively added were similar in size. The effect of V addition in Ni–Ti–B_4C–BN system on the size of ceramic particles is stronger than that of adding W, Al and Co [42,43].

Figure 7a,b shows the changes in reaction enthalpy (ΔH^0) and standard Gibbs free energy (ΔG^0) for the latent reactions in Ni–(V/Co)–Ti–B_4C–BN systems with the change of temperature, respectively. Equations (2)–(10) are the reactions between each reactant or some intermediate phases. Moreover, certain proportions of TiC and TiN were used to represent the TiCN, overcome the relative complexity of the TiCN thermodynamic data and ignore the effect of TiC+TiN on TiCN.
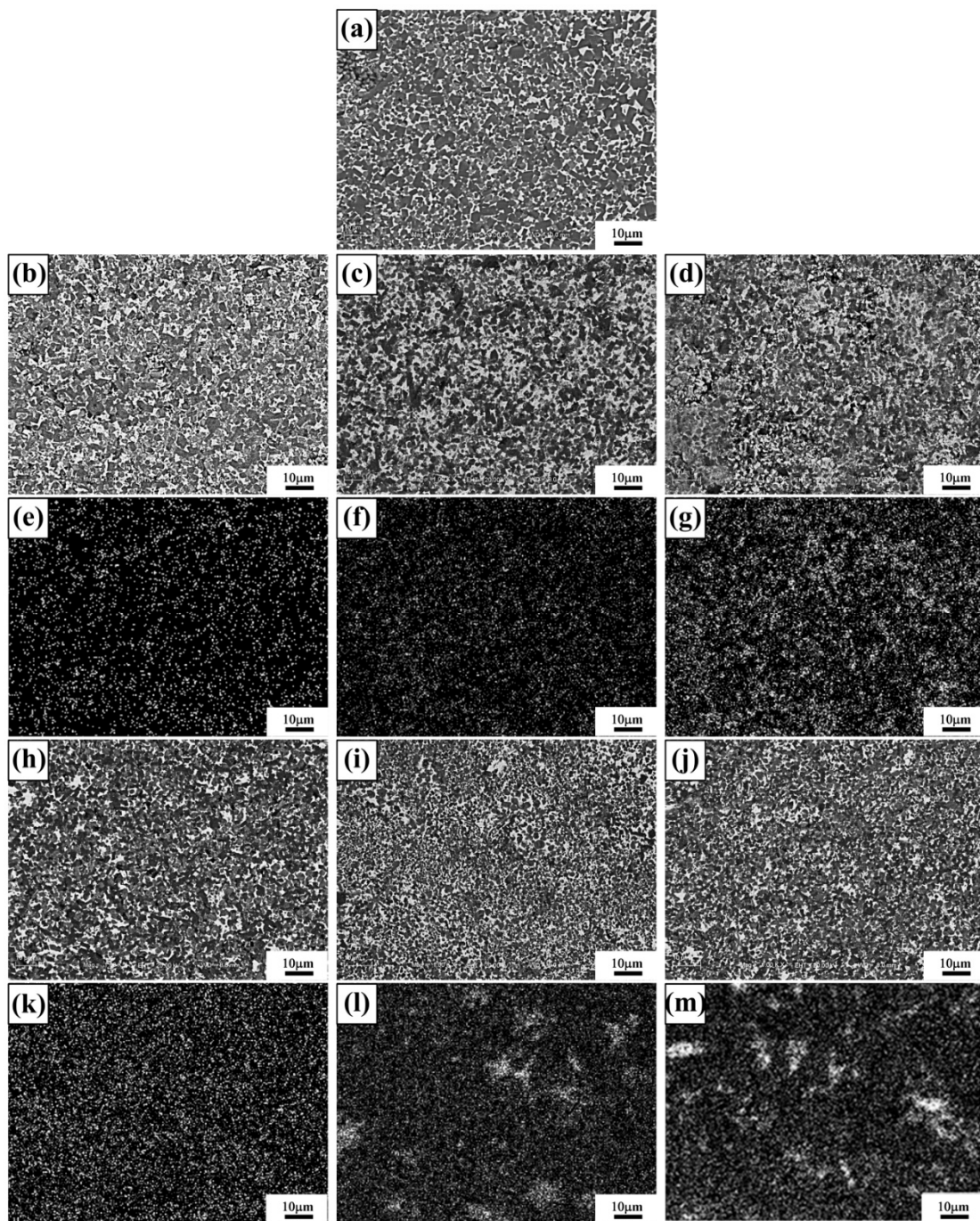
Figure 4. Microstructures of the (TiC$_x$N$_y$–TiB$_2$)/Ni cermets with different Co and V contents. (**a**) SEM images of (TiC$_x$N$_y$–TiB$_2$)/Ni cermets with 30 wt.% Ni. (**b**–**d**) and (**e**,**f**) SEM and EDS images of 70 wt.% (TiC$_x$N$_y$–TiB$_2$)/Ni cermets with 2, 5 and 8 wt.% Co, respectively. (**h**–**j**) and (**k**–**m**) SEM and EDS images of 70 wt.% (TiC$_x$N$_y$–TiB$_2$)/Ni cermets with 2, 5 and 8 wt.% V, respectively.
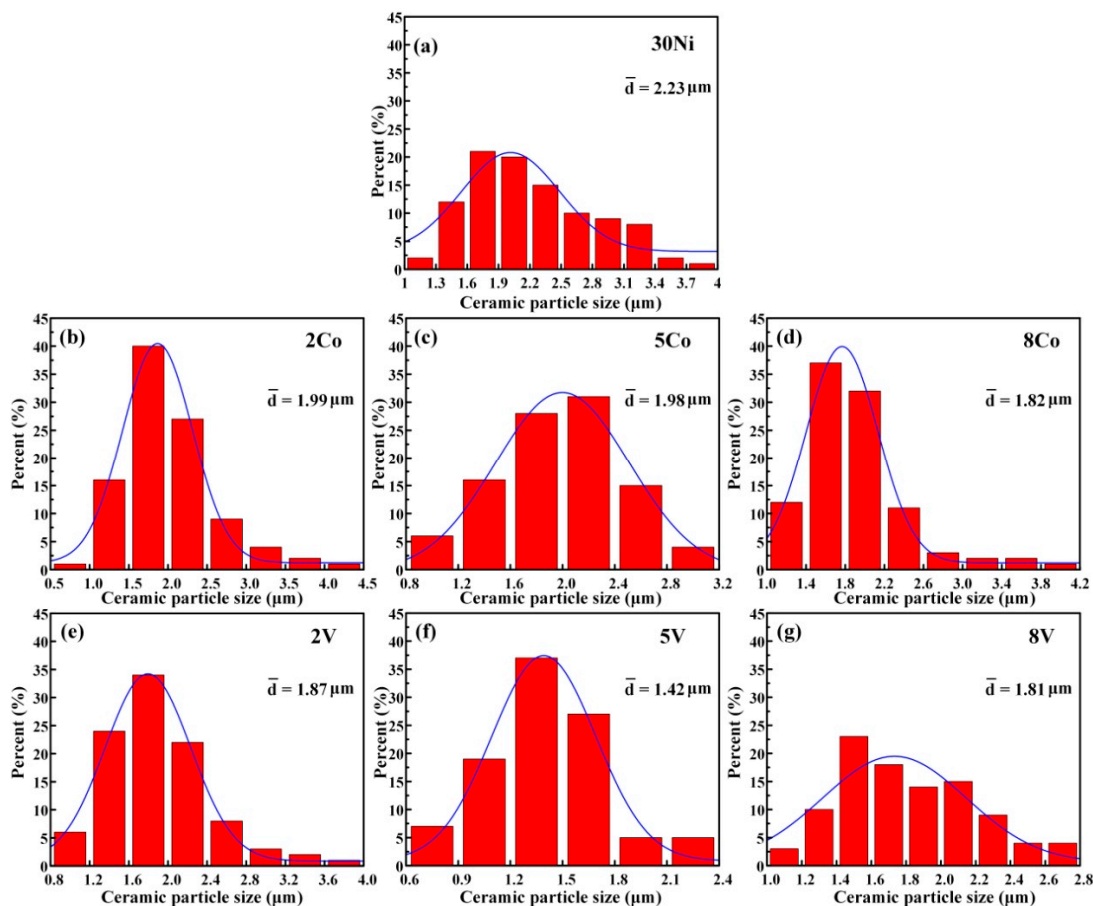
Figure 5. Size distribution diagrams of ceramic particles in the $(TiC_xN_y–TiB_2)/Ni$ cermets. (**a**) $(TiC_xN_y–TiB_2)/Ni$ cermets with 30 wt.% Ni. (**b–d**) 70 wt.% $(TiC_xN_y–TiB_2)/Ni$ cermets with 2, 5 and 8 wt.% Co, respectively. (**e–g**) 70 wt.% $(TiC_xN_y–TiB_2)/Ni$ cermets with 2, 5 and 8 wt.% V, respectively.

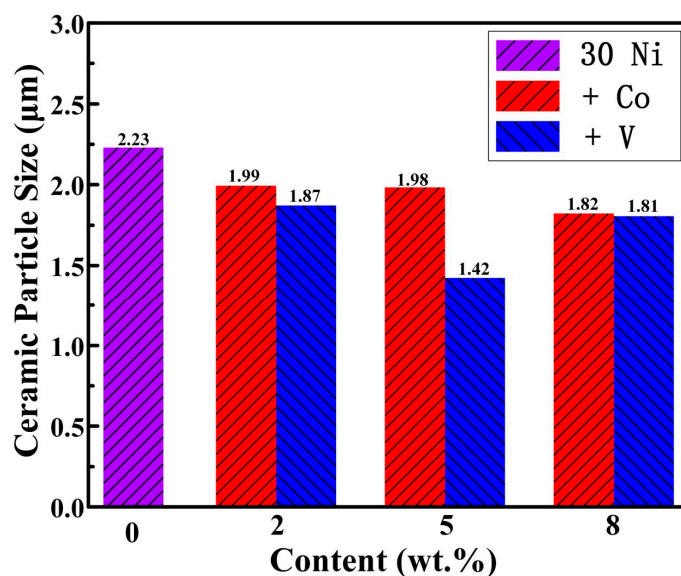**Figure 6.** Average size of ceramic particles with different Co and V contents.
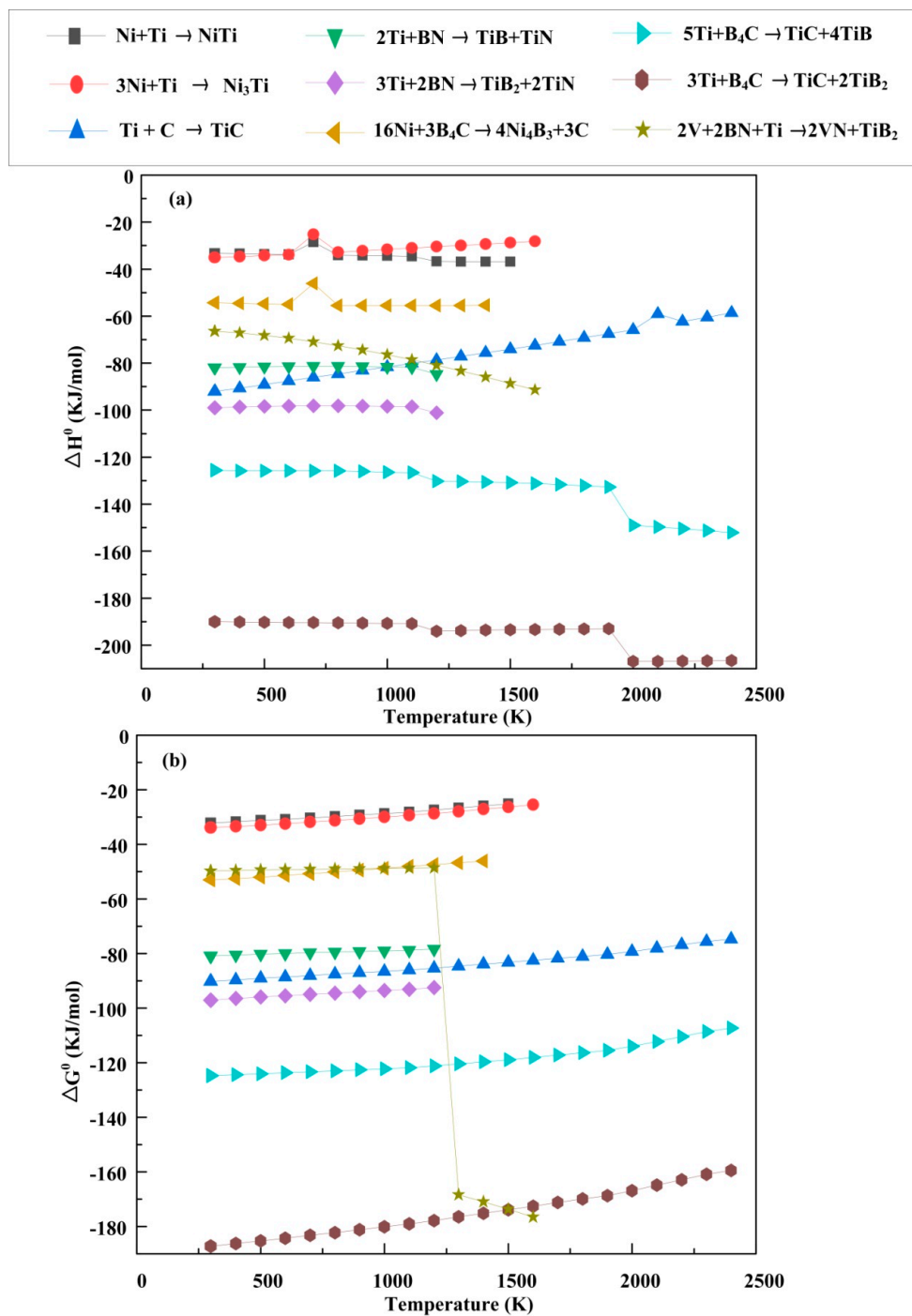
Figure 7. (**a**) ΔH^0 and (**b**) ΔG^0 of the latent reactions in Ni–(V/Co)–Ti–B_4C–BN systems with the change of temperature (K).

$$Ni + Ti \rightarrow NiTi \tag{2}$$

$$3Ni + Ti \rightarrow Ni_3Ti \tag{3}$$

$$Ti + C \rightarrow TiC \tag{4}$$

$$2Ti + BN \rightarrow TiB + TiN \tag{5}$$

$$3Ti + 2BN \rightarrow TiB_2 + 2TiN \tag{6}$$

$$16Ni + 3B_4C \rightarrow 4Ni_4B_3 + 3C \tag{7}$$

$$5Ti + B_4C \rightarrow TiC + 4TiB \tag{8}$$

$$3Ti + B_4C \rightarrow TiC + 2TiB_2 \tag{9}$$

$$2V + 2BN + Ti \rightarrow 2VN + TiB_2 \tag{10}$$
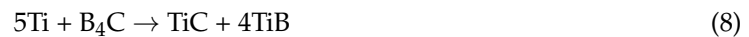
All of the reactions were thermodynamically feasible, with a negative Gibbs free energy exhibited in the calculated temperature range. Furthermore, the reaction enthalpy suggested that reactions (2)–(10) were all exothermal ($\Delta H^0 < 0$). Reaction (9) had the lowest reaction enthalpy and a far more negative standard Gibbs free energy, suggesting that TiC and TiB$_2$ were the most stable products and that this reaction had the largest thermodynamics driving force contract with other reactions. TiN and TiB were less stable products, while NiTi, Ni$_3$Ti and Ni$_4$B$_3$ were the most unstable intermediate products, as reactions (2), (3) and (7) showed relatively less heat release and a higher Gibbs free energy and ultimately transformed into more stable products. As Figure 7b shows, the Gibbs free energy of reaction (10) remained constant at first and dropped dramatically when the temperature exceeded 1200 °C, suggesting that VN was more stable under elevated temperatures.

Figure 8 shows the DTA curves of different contents of Co/V in Ni–Ti–B$_4$C–BN systems. Adding Co and V to the alloy had different effects on the reaction temperature of the system. Co played a role in dilution in the reaction system, so after the addition of Co, the reaction was delayed. With the addition of Co, the maximum combustion temperature continued to decrease, as shown in Figure 9. Although V participated in the reaction, a small added amount increased the maximum exothermic peak temperature. When the V content reached 8 wt.%, the amount of VN generated rose sharply, a large amount of heat was released and the reaction temperature of the system increased. Therefore, the reaction temperature of the system after the addition of V decreased first and then increased, as shown in Figure 9. The heat of fusion of V was larger than that of Co, so when the alloying element content was less than 5 wt.%, the reaction temperature of the alloy to which the V element was added decreased more than that of the Co element.
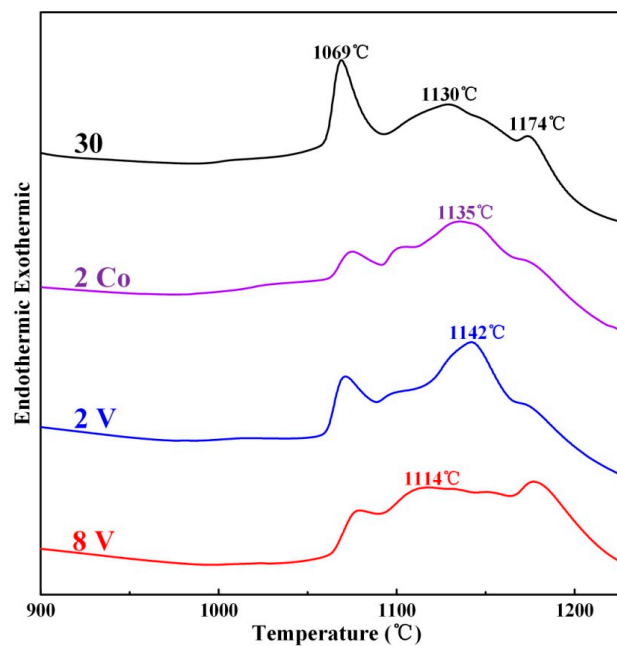

Figure 8. Differential thermal analysis (DTA) curves of different contents of Co/V in Ni–Ti–B$_4$C–BN systems.
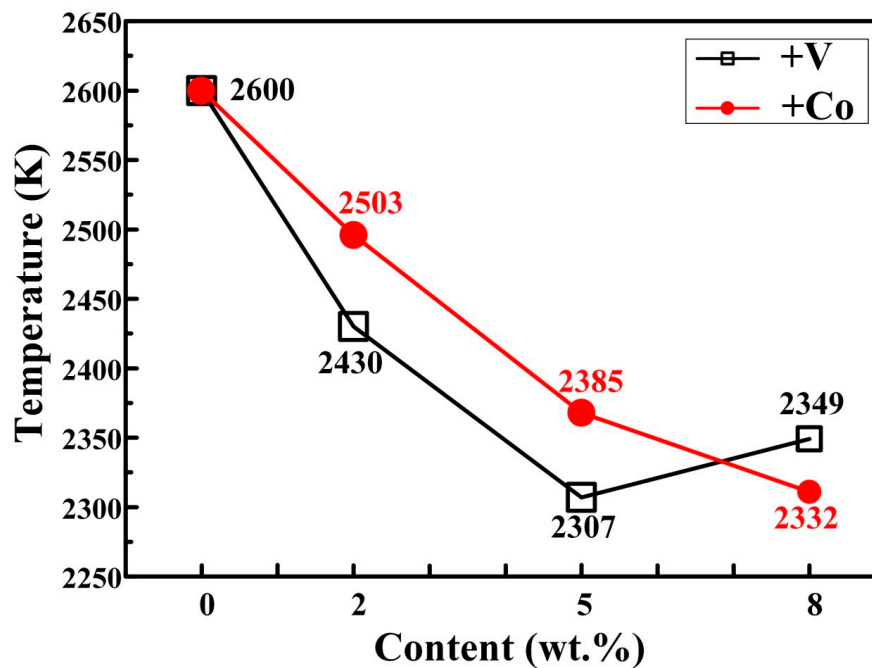
Figure 9. Combustion temperature curve of Ni–Ti–B$_4$C–BN systems with different Co/V contents.

The highest combustion temperature is an important factor in the growth of ceramic particles, and a low reaction temperature leads to a size reduction of ceramic particles in composites. Figure 9 shows the combustion temperature curve of Ni–Ti–B$_4$C–BN systems with different Co/V contents. The Co element did not participate in the SHS reaction and was a diluent; therefore, when the Co element was added, the combustion temperature continued to decrease. When the V content was no more than 5 wt.%, as the V content increased, the maximum combustion temperature decreased. When the content of V was less than 5 wt.%, the concentration of V was not sufficient to greatly promote the generation of VN. Therefore, V absorbed a large amount of heat during the reaction, resulting in a continuous decrease in the reaction temperature of the reaction system during the reaction. When the content of the added V continued to increase to 8 wt.%, V participated in the reaction, which was exothermic. This resulted in a higher temperature during the reaction than the maximum combustion temperature of the reaction in the system in which 5 wt.% of the alloying element V was added. Therefore, the average size of the ceramic particles in the cermets with 8 wt.% V content was larger than that with 5 wt.% V added. With the addition of W and Al, and the sizes of the ceramic particles continues to decrease due to the reduction of the maximum combustion temperature in the Wang's works and our previous works [42,43].

By analyzing the XRD, SEM and EDS of the Ni–Ti–B$_4$C–BN–Co/V system, the influence of V and Co on the reaction mechanism of Ni–Ti–B$_4$C–BN system could be established, as shown in Figure 10. In the Ni–Ti–B$_4$C–BN system, the solid-solid reactions between Ni and B$_4$C and between Ti and BN occurred first, respectively forming Ni$_2$B, Ni$_4$B$_3$ and C and TiN$_x$ and B. Ni then reacted with TiN$_x$ to form NiTi and Ni$_3$Ti. As the temperature increased, the Ni–B and Ni–Ti liquid phases formed between Ni$_2$B and Ni$_4$B$_3$ and between NiTi and Ni$_3$Ti, respectively. Once the liquid phases were formed, they rapidly spread on the surface of the unreacted particles, greatly promoting the dissolution of B, N and C atoms in the liquid phase and thereby forming a Ni–Ti–B–N–C liquid phase. When the concentrations of [Ti], [B], [C] and [N] in the liquid phase of Ni–Ti–B–N–C satisfied the thermodynamic conditions for the formation of TiB$_2$ and TiC$_x$N$_y$, the reaction formed TiB$_2$ and TiC$_x$N$_y$ and precipitated from the liquid phase. As shown in Figure 10a, Co did not participate in the reaction, but had an inhibitory effect on the synthesis process by diluting the reactant. Finally, a fraction of the Co atoms entered the Ni to form a solid solution in the matrix, while the remaining Co atoms were segregated around the interface between the ceramic particles. In the Ni–Ti–B$_4$C–BN–V systems, when the V

content was 5 wt.%, as shown in Figure 10b, the concentration of VN was not greatly promoted due to insufficient concentration; V acted only to refine the particles, and the ceramic particles were the smallest at this time. When the V content reached 8 wt.%, the increase in V concentration greatly promoted the generation of VN, the reaction temperature of the system increased and the size of the ceramic particles increased.
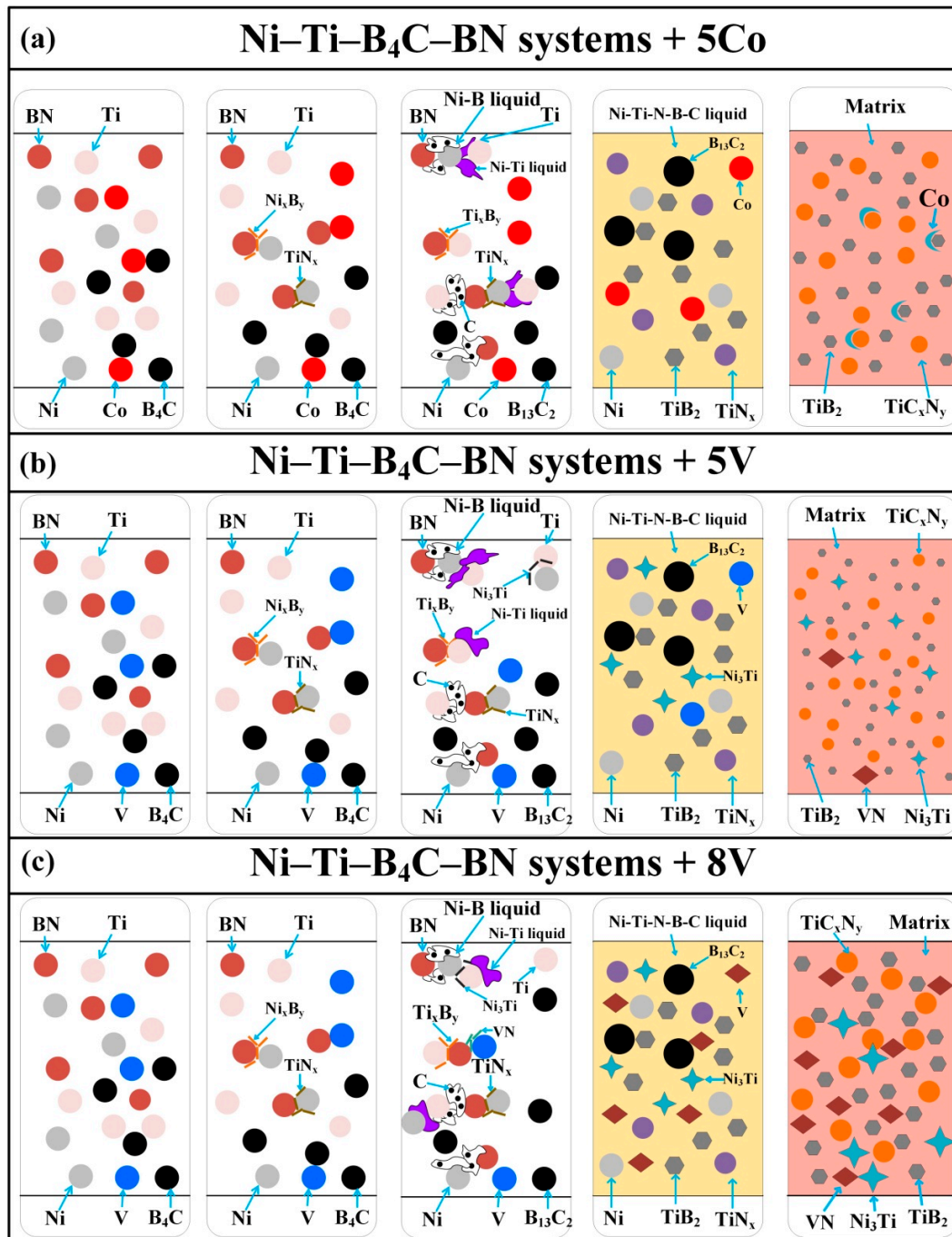

Figure 10. Reaction mechanism diagram of Ni–Ti–B$_4$C–BN systems (**a**), (**b**) and (**c**) are the reaction mechanisms of Ni–Ti–B$_4$C–BN systems with 5 wt.% Co, 5 wt.% V and 8 wt.% V, respectively.

Figure 11 shows the compressive engineering stress-strain curves for (TiC$_x$N$_y$–TiB$_2$)/(Ni+Co/V) cermets with different Co and V contents. The addition of Co and V elements resulted in a different degree of improvement in the mechanical properties of the cermets. Table 1 lists the hardness

and mechanical properties of $(TiC_xN_y–TiB_2)/Ni$ cermets with different Co and V contents. As the Co content increased, the relative density of the cermets increased first and then decreased. The addition of Co was beneficial to the wetting between ceramic particles and nickel, thus contributing to the densification of the cermets. With the Co content increased, the reaction temperature of the system decreased; the reduction of the reaction temperature was not conducive to densification. Therefore, when the Co content was 8 wt.%, the relative density was reduced. Figure 11a shows the compressive engineering stress-strain curves for $(TiC_xN_y–TiB_2)/(Ni+Co)$ cermets with different Co contents. With the increase in Co content from 0 to 5 wt.%, the ultimate compressive strength (σ_{UGS}) and fracture strain (ε_f) increased from 2.94 to 3.25 GPa and 2.9% to 3.25%, respectively. Then, as the Co content continued to increase, both σ_{UGS} and ε_f decreased. When the Co content was 5 wt.%, the hardness of the cermets reached the highest value of 1967 Hv. Impact toughness is an important property for brittle cermets [44,45]. The impact properties of $(TiC_xN_y–TiB_2)/(Ni+Co/V)$ cermets with different Co and V contents are shown in Table 1. As the Co content increased, the impact toughness of the cermets increased from 2.94 and 6.05 to 7.52 GPa. The addition of V reduced the impact properties of $(TiC_xN_y–TiB_2)/(Ni+V)$ cermets. The addition of Co strengthens the impact toughness of the $(TiC_xN_y–TiB_2)/Ni$ cermets, while the addition of V deteriorates it. Obviously, the addition of a small amount of Co promoted the wetting of ceramic particles and Ni was beneficial to the densification of the cermets, strengthened the interfacial bonding between the ceramic particles and Ni, improved the strength and hardness of the cermets, and reduced the density, strength and hardness when the amount of addition was too much.
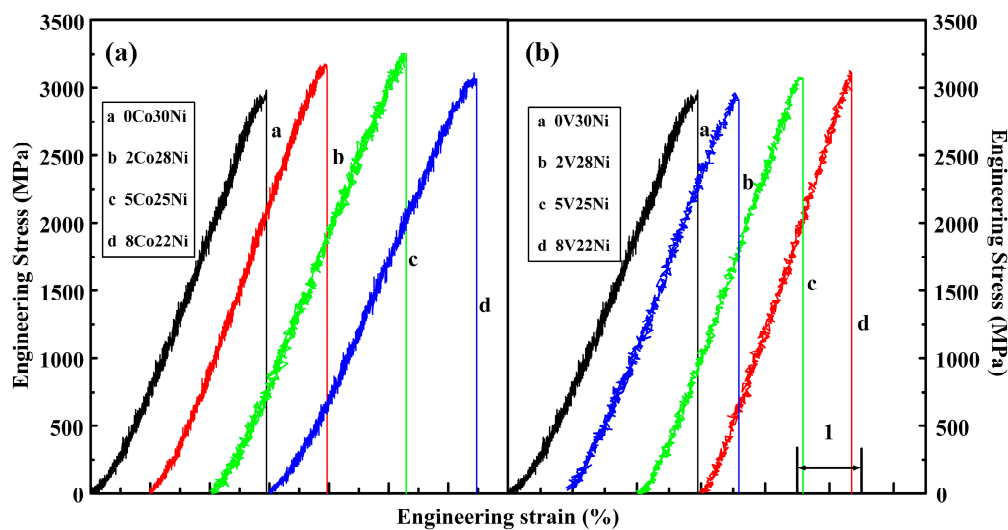

Figure 11. Compression engineering stress-strain curves of the $(TiC_xN_y–TiB_2)/Ni$ cermets. (**a**) $(TiC_xN_y–TiB_2)/Ni$ cermets with different Ni and Co contents. (**b**) $(TiC_xN_y–TiB_2)/Ni$ cermets with different Ni and V contents.

Table 1. Room-temperature compression properties, impact toughness, microhardness and density of $(TiC_xN_y–TiB_2)/Ni$ cermets with different Co and V contents.

Sample	Density			Hv	σ_{UGS} (GPa)	ε_f (%)	K_c (MPa·m$^{1/2}$)
	Theoretical Density (g/cm^3)	Measured Density (g/cm^3)	Relative Density (%)				
30 wt.% Ni	5.52	5.24	94.8	1561 ± 31	$2.94^{+0.5}_{-0.3}$	$2.9^{+0.6}_{-0.4}$	6.05 ± 0.25
28 wt.% Ni + 2Co	5.52	5.35	96.8	1759 ± 52	$3.17^{+0.8}_{-0.4}$	$3.0^{+1.3}_{-0.5}$	6.56 ± 0.18
25 wt.% Ni + 5Co	5.52	5.39	97.4	1967 ± 40	$3.25^{+0.6}_{-0.3}$	$3.3^{+0.7}_{-0.3}$	6.97 ± 0.31
22 wt.% Ni + 8Co	5.52	5.29	95.9	1914 ± 51	$3.07^{+0.4}_{-0.5}$	$3.5^{+0.9}_{-0.6}$	7.52 ± 0.33
28 wt.% Ni + 2V	5.48	5.34	97.4	1730 ± 25	$2.96^{+0.7}_{-0.9}$	$2.6^{+0.4}_{-0.7}$	5.76 ± 0.25
25 wt.% Ni + 5V	5.43	5.34	98.2	1760 ± 63	$3.07^{+0.3}_{-0.6}$	$2.6^{+0.8}_{-0.6}$	5.93 ± 0.16
22 wt.% Ni + 8V	5.38	5.28	98.2	1823 ± 45	$3.11^{+1.2}_{-0.9}$	$2.3^{+0.5}_{-0.9}$	5.65 ± 0.17

As the V content increased, the relative density of the $(TiC_xN_y–TiB_2)/(Ni+V)$ cermets increased continuously. Unlike the addition of the Co element, the relative density of the cermets with V added increased as the V content increased; when the V element reached a certain content, the relative density did not change. The hardness of the cermets increased as the V content increased. Figure 11b shows the compressive engineering stress–strain curves for $(TiC_xN_y–TiB_2)/(Ni+V)$ cermets with different V contents. As the V content increased, the σ_{UGS} of the cermets increased, while the ε_f decreased. When the content of V was 8 wt.%, the cermets had the highest compressive strength of 3.11 GPa and the minimum ε_f was 2.3%. The hardness of the cermets reached the maximum level. When the V content in the cermets reached 8 wt.%, there was a large amount of VN formation in the alloy system, and the ceramic content in the cermets increased, which led to a large increase in the strength and hardness of the $(TiC_xN_y–TiB_2)/(Ni+Co)$ cermets.

Figure 12 shows SEM images of the compression fractured surfaces for $(TiC_xN_y–TiB_2)/Ni$ cermets with 5 wt.% Co and V added. As indicated, in the $(TiC_xN_y–TiB_2)/Ni$ cermets without the addition of Co and V, most of the cracks propagated along the ceramics–Ni interface, while in the cermets with the addition of Co and V, there were no obvious cracks on the surface of the fracture. This indicates that the addition of Co and V in the cermets increased the bonding strength between the Ni and ceramic particles, thereby increasing the compressive strength and toughness of the cermets.
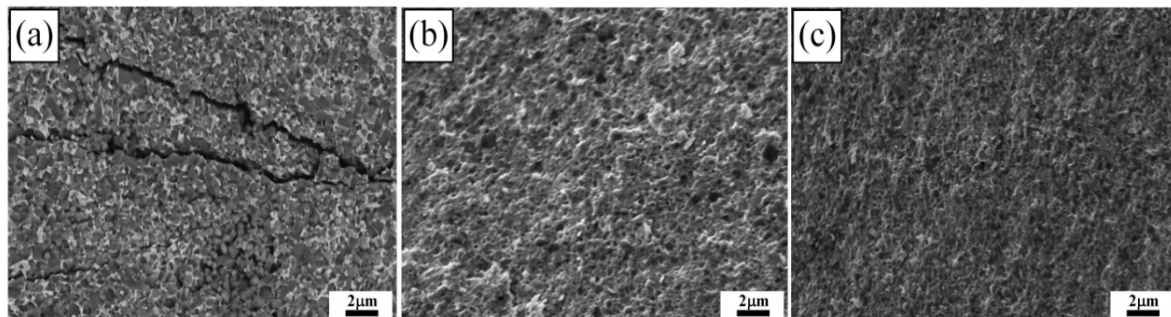

Figure 12. SEM images of the compression fractured surfaces for $(TiC_xN_y–TiB_2)/Ni$ cermets. (**a**) $(TiC_xN_y–TiB_2)/Ni$ cermets with no alloy element. (**b**) $(TiC_xN_y–TiB_2)/Ni$ cermets with 5 wt.% Co. (**c**) $(TiC_xN_y–TiB_2)/Ni$ cermets with 5 wt.% V.

Figure 13 shows variations of the (a) relative density, (b) microhardness, (c) ultimate compressive strength and (d) fracture strain of $(TiC_xN_y–TiB_2)/Ni$ cermets with different Co/V contents. The addition of Co was more effective than the addition of V for the ultimate compressive strength, the impact toughness and microhardness of the $(TiC_xN_y–TiB_2)/Ni$ cermets. The addition of the V element mainly refined the ceramic particles in the cermets; therefore, as the V content increased, the microhardness and ultimate compressive strength of the cermets increased. The addition of Co and V reduced the reaction temperature of the system, but the heat of fusion of V was 21.5 kJ/mol^{-1} higher than that of Co 16.06 kJ/mol^{-1}, so the reaction temperature of V was lower than that of Co. As the V content increased, the number of ceramic particles increased, which reduced the content of Ni in the cermets and reduced the shaping of the cermets. Hence, as the V content increased, the fracture strain of the cermets decreased. The following factors affected the influence of the addition of the Co element on the cermets. First, Co could form an infinite solid solution with Ni in the matrix. The more Co atoms dissolved in the Ni, the stronger the solid solution became. Second, as the Co content increased, the size of the cermets' ceramic particles decreased slightly. Therefore, when the Co content increased from 0 to 5 wt.%, the hardness and compressive strength of the cermets also gradually increased. Ultimately, the addition of Co promoted the wetting of ceramic particles and Ni and strengthened the interfacial bonding between the ceramic particles and Ni. However, when Co was continuously added to the Ni–Co–Ti–B$_4$C–BN systems to 8 wt.%, the density of the cermets decreased, resulting in a decrease in performance of the cermets.
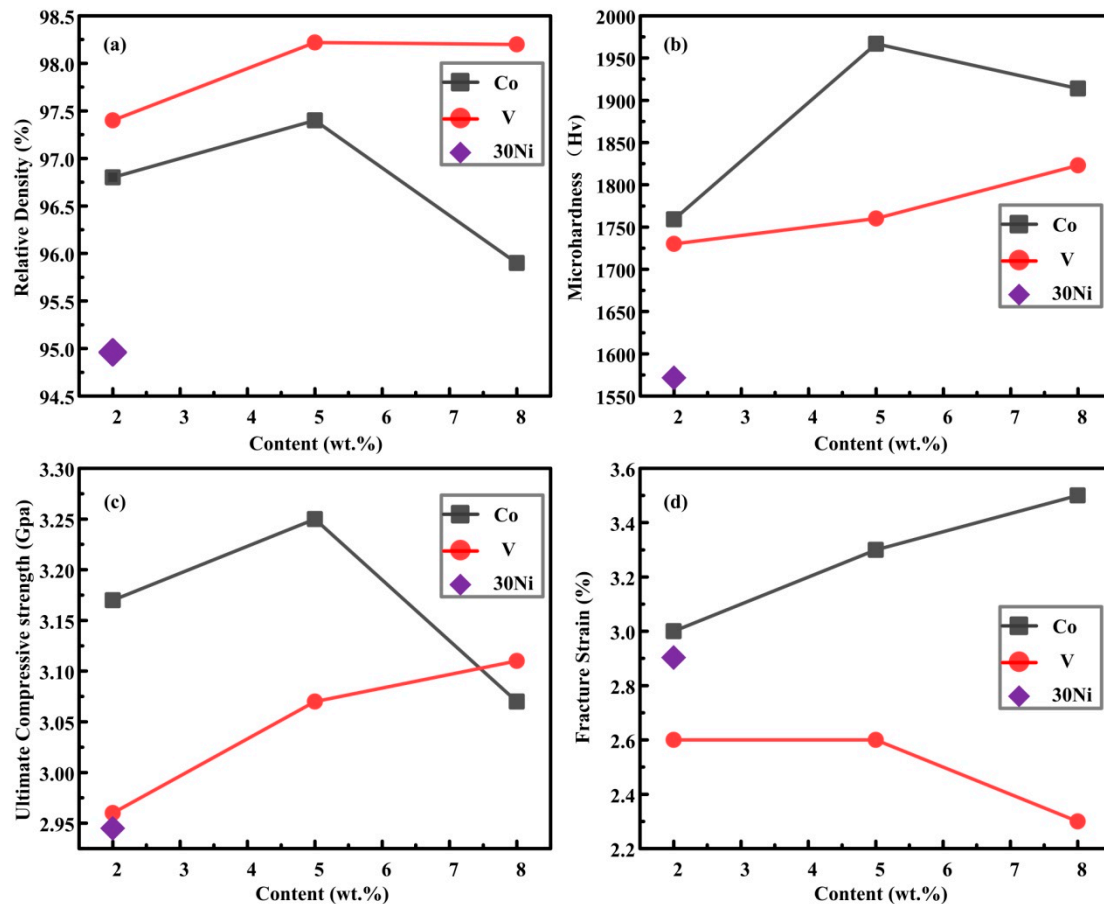
Figure 13. Variations of (**a**) relative density, (**b**) microhardness (Hv), (**c**) ultimate compressive strength σ_{UGS} and (**d**) fracture strain ε_f of (TiC$_x$N$_y$–TiB$_2$)/Ni cermets with different Co/V contents.

4. Conclusions

Microstructure and mechanical properties of (TiCxNy–TiB2)/Ni cermets with different Co and V contents (2, 5 and 8 wt.%) fabricated by combustion synthesis and hot press consolidation were studied. The addition of Co and V elements refined the ceramic particles to different degrees. Co did not participate in the reaction, but had an inhibitory effect on the synthesis process by diluting the reactant. When the V content was 5 wt.%, V acted only to refine the particles, and the ceramic particles were the smallest at this time. When the V content reached 8 wt.%, the increase in V concentration greatly promoted the generation of VN, the reaction temperature of the system increased and the size of the ceramic particles increased. The heat of fusion of V was higher than that of Co, so the decrease in the temperature and the refinement effect on the ceramic particles of the V element were more significant. The cermets with 5 wt.% Co possessed the best comprehensive properties: the highest hardness (1967 Hv), a superior compression strength (3.25 GPa) and a higher fracture strain (3.3%), which are 406 Hv, 0.31GPa and 0.4% higher than those of the unalloyed cermets. Correspondingly, when the V content was 8 wt.%, those three values reached 1823 Hv, 3.11 GPa and 2.3%, respectively. The addition of Co acted as a fine-grained strengthening and solid solution strengthening, and Co promoted the wetting of ceramic particles and Ni and strengthened the interfacial bonding between the ceramic particles and Ni. Furthermore, as the V content increased to 8 wt.%, the number of ceramic particles increased, which reduced the Ni content and thereby the shaping of the cermets. Therefore, the addition of Co is more significant than the addition of V to the mechanical properties of the cermets.

Author Contributions: Funding Acquisition, X.L. and F.Q.; Conceptualization, X.L. and F.Q.; Investigation, X.D., H.Y. and Y.W.; Writing: Original Draft Preparation, X.D.; Formal Analysis, F.Q. and H.Y.; Data Curation, X.L.; Writing: Review and Editing, X.L.

Conflicts of Interest: The authors declare no conflict of interest.

References

1.　Zhan, L.; Shen, P.; Jiang, Q.C. The mechanism of combustion synthesis of $(TiC_xN_y–TiB_2)$/Ni from a Ni–Ti–C–BN system. *Powder Technol.* **2011**, *205*, 52–60. [CrossRef]

2.　Zhan, L.; Shen, P.; Yang, Y.F.; Zhang, J.; Jiang, Q.C. Self-propagating high-temperature synthesis of $TiC_xN_y–TiB_2$ ceramics from a Ti–B_4C–BN system. *Int. J. Refract. Met. H* **2009**, *27*, 829–834. [CrossRef]

3.　Xu, Q.Z.; Ai, X.; Zhao, J.; Zhang, H.S.; Qin, W.Z.; Gong, F. Effect of heating rate on the mechanical properties and microstructure of Ti(C,N)-based cermets. *Mater. Sci. Eng. A* **2015**, *628*, 281–287. [CrossRef]

4.　Zhai, W.; Song, X.; Li, T.; Yu, B.X.; Lu, W.H.; Zeng, K.Y. Ti reactive sintering of electrically conductive Al_2O_3–TiN composite: Influence of Ti particle size and morphology on electrical and mechanical properties. *Materials* **2017**, *10*, 1348. [CrossRef]

5.　Shu, S.L.; Yang, H.Y.; Tong, C.Z.; Qiu, F. Fabrication of TiC_x-TiB_2/Al composites for application as a heat sink. *Materials* **2016**, *9*, 642. [CrossRef] [PubMed]

6.　Song, J.P.; Huang, C.Z.; Lv, M.; Zou, B.; Wang, S.Y.; Wang, J.; An, J. Effects of TiC content and melt phase on microstructure and mechanical properties of ternary TiB_2-based ceramic cutting tool materials. *Mater. Sci. Eng. A* **2014**, *605*, 137–143. [CrossRef]

7.　Zhao, G.L.; Huang, C.Z.; Liu, H.L.; Zou, B.; Zhu, H.T.; Wang, J. Microstructure and mechanical properties of hot pressed TiB_2–SiC composite ceramic tool materials at room and elevated temperatures. *Mater. Sci. Eng. A* **2014**, *606*, 108–116. [CrossRef]

8.　Xu, Q.Z.; Zhao, J.; Ai, X.; Qin, W.Z.; Wang, D.W.; Huang, W.M. Effect of Mo_2C/(Mo_2C+WC) weight ratio on the microstructure and mechanical properties of Ti(C,N)-based cermet tool materials. *J. Alloy. Compd.* **2015**, *649*, 885–890. [CrossRef]

9.　Zhao, Q.; Liang, Y.H.; Zhang, Z.H.; Li, X.J.; Ren, L.Q. Study on the impact resistance of bionic layered composite of TiC-TiB_2/Al from Al-Ti-B_4C system. *Materials* **2016**, *9*, 708. [CrossRef] [PubMed]

10.　Qiu, F.; Chu, J.G.; Hu, W.; Lu, J.B.; Li, X.D.; Han, Y.; Jiang, Q.C. Study of effect of Zr addition on the microstructures and mechanical properties of $(TiC_x–TiB_2)$/Cu composites by combustion synthesis and hot press consolidation in the Cu–Ti–B_4C–Zr system. *Mater. Res. Bull.* **2015**, *70*, 167–172. [CrossRef]

11.　Yang, C.; Guo, H.; Mo, D.G.; Qu, S.G.; Li, X.Q.; Zhang, W.W.; Zhang, L.C. Bulk TiB_2-based ceramic composites with improved mechanical property using Fe–Ni–Ti–Al as a sintering aid. *Materials* **2014**, *7*, 7105–7117. [CrossRef] [PubMed]

12.　Bazhin, P.M.; Stolin, A.M.; Konstantinov, A.S.; Kostitsyna, E.V.; Ignatov, A.S. Ceramic Ti-B composites synthesized by combustion followed by high-temperature deformation. *Materials* **2016**, *9*, 1027. [CrossRef] [PubMed]

13.　Deng, J.X.; Zhang, H.; Wu, Z.; Lian, Y.S.; Xing, Y.Q.; Li, S.P. Unlubricated friction and wear behaviors of Al_2O_3/TiC ceramic cutting tool materials from high temperature tribological tests. *Int. J. Refract. Met. Hard Mater.* **2012**, *35*, 17–26.

14.　Cao, X.Z.; Wang, C.; Shi, L.H.; Yang, H.; Xue, X.X.; Li, H.T. Effect of Ni addition on pressureless sintering of tungsten diboride. *Int. J. Refract. Met. Hard Mater.* **2013**, *41*, 597–602. [CrossRef]

15.　Liang, Y.H.; Zhao, Q.; Han, Z.W.; Zhang, Z.H.; Li, X.J.; Ren, L.Q. Microstructures and Wear Behavior of the TiC Ceramic Particulate Locally Reinforced Steel Matrix Composites from a Cu–Ti–C System. *ISIJ. Int.* **2015**, *55*, 319–325. [CrossRef]

16.　Qiu, F.; Gao, X.; Tang, J.; Gao, Y.Y.; Shu, S.L.; Han, X.; Li, Q.; Jiang, Q.C. Microstructures and tensile properties of Al–Cu matrix composites reinforced with nano-sized SiC_p fabricated by semisolid stirring process. *Metals* **2017**, *7*, 49. [CrossRef]

17.　Wang, Y.H.; Kou, Z.L.; Liu, Y.J.; Liu, F.M.; He, D.W. Ti (C,N)-based cermets sintered under high pressure. *Int. J. Refract. Met. Hard Mater.* **2016**, *54*, 203–209. [CrossRef]

18. Zhao, X.R.; Zuo, D.W.; Zhang, M.X.; Xu, F.; Feng, S.S. In situ production of ultra-fine Ti(C,N)-TiB$_2$-Co cermets by reactive hot processing from the Co–Ti–C–BN system. *Int. J. Refract. Met. Hard Mater.* **2016**, *55*, 1–10. [CrossRef]

19. Liu, C.; Lin, N.; He, Y.H. Influence of Mo$_2$C and TaC additions on the microstructure and mechanical properties of Ti(C,N)-based cermets. *Ceram. Int.* **2016**, *42*, 3569–3574. [CrossRef]

20. Zhao, G.L.; Huang, C.Z.; He, N.; Liu, H.L.; Zou, B. Microstructure and mechanical properties at room and elevated temperatures of reactively hot pressed TiB$_2$-TiC-SiC composite ceramic tool materials. *Ceram. Int.* **2016**, *42*, 5353–5361. [CrossRef]

21. Yang, W.Q.; Xing, L.L.; Lin, T.S.; He, P.; Lin, J.C.; Ma, X.F. Microstructural evolution and growth/degradation behavior of in situ TiB whiskers in ZrB$_2$-SiC joints using Ti/Ni/Ti filler. *J. Alloy. Compd.* **2018**, *744*, 124–131. [CrossRef]

22. Wolfrum, A.K.; Matthey, B.; Michaelis, A.; Herrmann, M. On the stability of c-BN-reinforcing particles in ceramic matrix materials. *Materials* **2018**, *11*, 255. [CrossRef] [PubMed]

23. Zhao, Q.; Liang, Y.H.; Liu, Q.P.; Zhang, Z.H.; Yu, Z.L.; Ren, L.Q. Study on the mechanical properties of bionic coupling layered B$_4$C/5083Al composite materials. *Materials* **2018**, *11*, 680. [CrossRef] [PubMed]

24. Feng, L.C.; Guan, P.F.; Yu, X.M.; He, Y.Q. Microstructure and properties of thermal electrode material Si$_3$N$_4$–MoSi$_2$ composite ceramics. *Materials* **2018**, *11*, 986. [CrossRef] [PubMed]

25. Qiu, F.; Han, Y.; Cheng, A.; Lu, J.B.; Jiang, Q.C. Effect of Cr Content on the Compression Properties and Abrasive Wear Behavior of the High-Volume Fraction (TiC-TiB$_2$)/Cu Composites. *Acta. Metall. Sin (Engl. Lett.)* **2014**, *27*, 951–956. [CrossRef]

26. Lin, J.; Yang, Y.H.; Zhang, H.A.; Gong, J.F. Effects of CNTs content on the microstructure and mechanical properties of spark plasma sintered TiB$_2$-SiC ceramics. *Ceram. Int.* **2017**, *43*, 1284–1289. [CrossRef]

27. Gao, Y.Y.; Qiu, F.; Shu, S.L.; Wang, L.; Chang, F.; Hu, W.; Han, X.; Li, Q.; Jiang, Q.C. Mechanical properties and abrasive wear behaviors of in situ nano-TiC$_x$/Al-Zn-Mg-Cu composites fabricated by combustion synthesis and hot press consolidation. *Arch. Civ. Mech. Eng.* **2018**, *18*, 179–187. [CrossRef]

28. Liu, C.X.; Zhang, J.H.; Zhang, X.H.; Sun, J.L. Fabrication of Al$_2$O$_3$/TiB$_2$/AlN/TiN and Al$_2$O$_3$/TiC/AlN composites. *Mater. Sci. Eng. A* **2007**, *465*, 72–77.

29. Deng, Y.; Deng, L.; Xiong, X.; Ye, J.W.; Li, P.P. Physical properties and microstructure of Ti(CN)-based cermets with different WC particle size. *Mater. Sci. Eng. A* **2014**, *616*, 352–356. [CrossRef]

30. Zhang, D.D.; Bai, F.; Wang, Y.; Wang, J.G.; Wang, W.Q. Grain refinement and mechanical properties of Cu–Cr–Zr alloys with different nano-sized TiC$_p$ addition. *Materials* **2017**, *10*, 919. [CrossRef] [PubMed]

31. Huang, L.M.; Luo, L.M.; Cheng, J.G.; Zhu, X.Y.; Wu, Y.C. The influence of TiB$_2$ content on microstructure and properties of W-30Cu composites prepared by electroless plating and powder metallurgy. *Adv. Powder Technol.* **2015**, *26*, 1058–1063. [CrossRef]

32. Xu, Q.Z.; Ai, X.; Zhao, J.; Qin, W.Z.; Wang, Y.T.; Gong, F. Comparison of Ti(C,N)-based cermets processed by hot-pressing sintering and conventional pressureless sintering. *J. Alloy. Compd.* **2015**, *619*, 538–543. [CrossRef]

33. Xu, Q.Z.; Ai, X.; Zhao, J.; Gong, F.; Pang, J.M.; Wang, Y.T. Effects of metal binder on the microstructure and mechanical properties of Ti(C,N)-based cermets. *J. Alloy. Compd.* **2015**, *644*, 663–672. [CrossRef]

34. Li, P.; Zhou, W.C.; Zhu, J.K.; Luo, F.; Zhu, D.M. Influence of TiB$_2$ content and powder size on the dielectric property of TiB$_2$/Al$_2$O$_3$ composites. *Scripta. Mater.* **2009**, *60*, 760–763. [CrossRef]

35. David Raja Selvam, J.; Dinaharan, I. In situ formation of ZrB$_2$ particulates and their influence on microstructure and tensile behavior of AA7075 aluminum matrix composites. *Int. J. Eng. Sci.* **2017**, *20*, 187–196.

36. Toozandehjani, M.; Matori, K.A.; Ostovan, K.A.; Aziz, S.A.; Mamat, M.S. Effect of milling time on the microstructure, physical and mechanical properties of Al-Al$_2$O$_3$ nanocomposite synthesized by ball milling and powder metallurgy. *Materials* **2017**, *10*, 1232. [CrossRef] [PubMed]

37. Tun, K.S.; Wong, W.L.E.; Nguyen, Q.B.; Gupta, M. Tensile and compressive responses of ceramic and metallic nanoparticle reinforced Mg composites. *Materials* **2013**, *6*, 1826–1839. [CrossRef] [PubMed]

38. Qiu, F.; Tong, H.T.; Gao, Y.Y.; Dong, B.X.; Li, Q.; Jiang, Q.C. Microstructures and compressive properties of al matrix composites reinforced with bimodal hybrid in-situ nano-/micro-sized tic particles. *Materials* **2018**, *11*, 1824. [CrossRef] [PubMed]

39.   Radishevskaya, N.; Lepakova, O.; Karakchieva, N.; Nazarova, A.; Afanasiev, N.; Godymchuk, N.; Gusev, A. Self-propagating high temperature synthesis of TiB$_2$-MgAl$_2$O$_4$ composites. *Metals* **2017**, *7*, 295. [CrossRef]

40.   Korosteleva, E.N.; Korzhova, V.V.; Krinitcyn, M.G. Sintering behavior and microstructure of TiC-Me composite powder prepared by SHS. *Metals* **2017**, *7*, 290. [CrossRef]

41.   Wang, Y.W.; Qiu, F.; Shu, S.L.; Lu, J.B.; Jiang, Q.C. Effect of Ni content on the compression properties and abrasive wear behavior of the(TiB$_2$–TiC$_x$N$_y$)/Ni composites. *Int. J. Refract. Met. H* **2012**, *34*, 8–12. [CrossRef]

42.   Wang, Y.W.; Shu, S.L.; Qiu, F.; Zhou, D.S.; Wang, J.G.; Jiang, Q.C. Effect of W content on the compression properties and abrasive wear behavior of the (TiB$_2$–TiC$_x$N$_y$)/(Ni+W) composites. *Mater. Des.* **2013**, *45*, 286–291. [CrossRef]

43.   Qiu, F.; Zuo, R.; Shu, S.L.; Wang, Y.W.; Jiang, Q.C. Effect of Al addition on the microstructures and compression properties of (TiC$_x$N$_y$–TiB$_2$)/Ni composites fabricated by combustion synthesis and hot press. *Powder Tech.* **2015**, *286*, 716–721. [CrossRef]

44.   Ghidelli, M.; Sebastiani, M.; Johanns, K.E.; Pharr, G.M. Effects of indenter angle on micro-scale fracture toughness measurement by pillar splitting. *J. Am. Ceram. Soc.* **2017**, *100*, 5731–5738. [CrossRef]

45.   Hu, W.Q.; Huang, Z.Y.; Cai, L.P.; Lei, C.; Zhai, H.X.; Wo, S.S.; Li, X.K. In-situ TiC and γ-Ni3(Al,Ti) triggered microstructural modification and strengthening of Ni matrix composite by reactive hot-press sintering pure Ni and Ti2AlC precursor. *J. Alloy. Compd.* **2018**, *747*, 1043–1052. [CrossRef]